

Local law-of-the-wall in complex topography: a confirmation from wind tunnel experiments

S. Besio, A. Mazzino and C.F. Ratto

INFN - National Institute for the Physics of Matter,
Department of Physics, Genova University, Genova (Italy).

October 24, 2018

Abstract

It is well known that in a neutrally-stratified turbulent flow in a deep constant-stress layer above a flat surface, the variation of the mean velocity with respect to the distance from the surface obeys the logarithmic law (the so-called “law-of-the-wall”). More recently, the same logarithmic law has been found also in the presence of non flat surfaces. It governs the dynamics of the mean velocity (i.e. all the smaller scales are averaged out) and involves renormalized effective parameters. Recent numerical simulations analyzed by the authors of the present Letter show that a more intrinsic logarithmic shape actually takes place also at smaller scales. Such a generalized law-of-the-wall involves effective parameters smoothly depending on the position along the underlying topography. Here, we present wind tunnel experimental evidence confirming and corroborating this new-found property. New results and their physical interpretation are also presented and discussed.

PACS: 83.10.Ji – 47.27.Nz – 92.60.Fm Boundary layer flows, Near wall turbulence

In the realm of boundary layer flows over complex topography, much effort has been devoted in the last few years to investigate both the detailed form of the surface pressure perturbation arising from the interaction between the shear flow and the underlying topography (see, e.g., Refs. [1, 2, 3]) and its link with the effective parameters describing the large (asymptotic) scale dynamics (see, e.g., Refs. [4, 5]). The latter regime is selected by observing the flow far enough from the surface and, furthermore, considering solely the mean velocity. It is thus clear that with this approach all information on the dynamics at smaller scale becomes completely lost.

Unlike what happens for the large-scale (asymptotic) dynamics, the description and understanding of statistical properties of flows at ‘intermediate’ scales (a regime which we refer to as “pre-asymptotic”, following Ref. [6]) seems strongly inadequate. Such regime actually attracts much attention in various applicative domains ranging from wind engineering (e.g., for the safe design and siting of buildings), environmental sciences (e.g., for the simulation of air pollution dispersion) and wind energy exploitation (e.g., for the selection of areas of enhanced wind speed for the economic siting of wind turbines).

This almost unexplored regime is the main concern of the present Letter. A first step in the understanding of the pre-asymptotic dynamics has been done by the present authors in a very recent work [6], where the analysis of simulations of Navier-Stokes flow fields [4] over two-dimensional sinusoidal topographies has been performed. More precisely, in the case-studies considered, topography takes a sinusoidal modulation of wavelength λ (along the x -direction, for the sake of simplicity) and amplitude H , its surface having an uniform roughness z_0 (with $z_0 \ll H$). Here, the dominant process governing the dynamics is the interaction between the shear flow and the underlying topography, the effect of which gives rise to a surface pressure perturbation [2]. Such perturbation has a depth of the order of H and a downwind phase shift with respect to the topography. The latter is the cause of a net force on the flow, acting in the opposite direction of the flow itself: thus, an enhanced (with respect to the case of flat terrain) transfer of momentum towards the surface takes place.

Far enough from the surface, the averaged (over the periodicity box of size λ) flow will ‘see’ an ‘effective flat surface’ over which the ‘basic’ logarithmic law (the well known “law-of-the-wall” relative to flows over flat terrain [7]) is restored but now with larger (again with respect to the flat case) effective parameters u_\star^{eff} , and z_0^{eff} [4], on account of the enhanced flux of momentum towards the surface originated by the aforesaid shear-flow – topography interaction.

In Ref. [6], we pointed out for the first time – as far as we know – that at least in the analyzed WM93 data-set [4], a generalized law-of-the-wall, is observed:

$$U(x, z) = \frac{u_\star^{\text{eff}}(x)}{k} \ln \left(\frac{z}{z_0^{\text{eff}}(x)} \right) \quad \text{for} \quad z > H \quad (1)$$

where U is the velocity field, x is the horizontal position, z is the height above the terrain, and k is the von Kármán constant which we will take as 0.4. Notice that the effective parameters, $u_\star^{\text{eff}}(x)$ and $z_0^{\text{eff}}(x)$, show a dependence on x at scales of the order of λ (i.e. the flow ‘sees’ some details of the topography and not only its total cumulative effects). This is precisely the pre-asymptotic regime already defined in Ref. [6].

In the present Letter, our main goal will be to provide a first experimental assessment confirming and corroborating the scenario outlined in Ref. [6]. In fact, the main trouble of numerical simulations of Navier-Stokes equations is that the impact on the results of

the closure schemes, through which small scale dynamics is accounted for, cannot be fully controlled [4]. An experimental confirmation is thus desirable.

To start our analysis, we briefly describe the experimental set-up relative to the wind tunnel experiment performed by Gong *et al* in Ref. [8]. Details on the description of the wind tunnel facility and the basic data acquisition and analysis system are given also in Ref. [9]. The experiment was conducted in the AES (Atmospheric Environment Service, Toronto, Canada) meteorological wind tunnel, which has a working volume of $2.44\text{ m} \times 1.83\text{ m} \times 18.29\text{ m}$ (w \times h \times l). The wave model consisted of sixteen sinusoidal waves with wavelength $\lambda \sim 610\text{ mm}$ and through-to-crest height $H \sim 96.5\text{ mm}$ and was placed with its leading edge at distance $d \sim 6.1\text{ m}$ downstream from a honeycomb located at the downstream end of the contraction region. The topography can be thus considered as a fraction of the ideal topography described by:

$$h(x, y) = H \sin^2 \left(\frac{\pi x}{\lambda} \right) \quad (2)$$

where y is the perpendicular-to- x -axis direction coordinate.

Two surface roughnesses were considered, corresponding to the natural foam surface (hereafter “smooth case”) and to a carpet cover (“rough case”), respectively. For the smooth case, velocity profile measurements gave $z_0 \sim 0.03\text{ mm}$, while for the rough case $z_0 \sim 0.40\text{ mm}$. The flow was neutrally stratified and can be considered as a perturbation to a stationary horizontally homogeneous infinitely deep unidirectional constant-stress-layer flow above a plane surface of uniform roughness, z_0 . Thus, this basic flow should have a logarithmic mean velocity profile, $U(z) = (u_*/\kappa) \ln(z/z_0)$. The values of u_* were $\sim 0.43\text{ m/s}$ and $\sim 0.62\text{ m/s}$ for the smooth and the rough case, respectively. The free-stream velocity, U_0 , at approximately 1 m above the floor of the tunnel, was set to about 10 m/s during the measurements both in the smooth and in the rough case. The boundary layer height, h_B , was evaluated to be $\sim 600\text{ mm}$. The rotation of the flow with the height, produced in the numerical simulations [4] by the Coriolis force, is obviously not present in the wind tunnel experiment and thus the flow is parallel to the x -axis at all elevations.

Measurements taken over the crests along the hills showed that the flow reached an almost periodic state quite rapidly, after the 3rd or 4th wave. Thus, the perturbed velocity profiles, $U(x, z)$, were measured at selected downstream locations between the 11th and 12th wave crests and a very good agreement between the profiles over these two crests was confirmed. This topography can be thus considered as a good approximation to a two-dimensional topography whose shape is described by Eq. (2)

In order to compare the numerical simulations analyzed in Ref. [6] with the results from the wind tunnel experiments here shortly described, we used the same approach as by Finardi *et al.* [10] and Canepa *et al.* [11]. Accordingly, noticing that in both cases here

considered $U_0 \sim 10 \text{ m/s}$, we have kept the speeds (including the friction velocities, u_*) unchanged, while the wind tunnel lengths (and times) have been multiplied by $\lambda_W/\lambda_G \sim 1000/0.6096 \sim 1640$, where λ_W and λ_G are the wavelengths in the Wood numerical simulations and in the Gong experiment, respectively. With this change of scale, $h_B \sim 1000 \text{ m}$ and $\lambda \sim 1000 \text{ m}$ in both cases, while the roughness lengths become $\sim 0.05 \text{ m}$ (smooth case) and $\sim 0.66 \text{ m}$ (rough case), to be compared with the value of $\sim 0.16 \text{ m}$ of the numerical simulations. The hill height, H , becomes $\sim 158 \text{ m}$, to be compared with the values 20 m , 100 m and 250 m in the Wood numerical experiments.

The first point to emphasize is that logarithmic laws described by (1) are evident also in

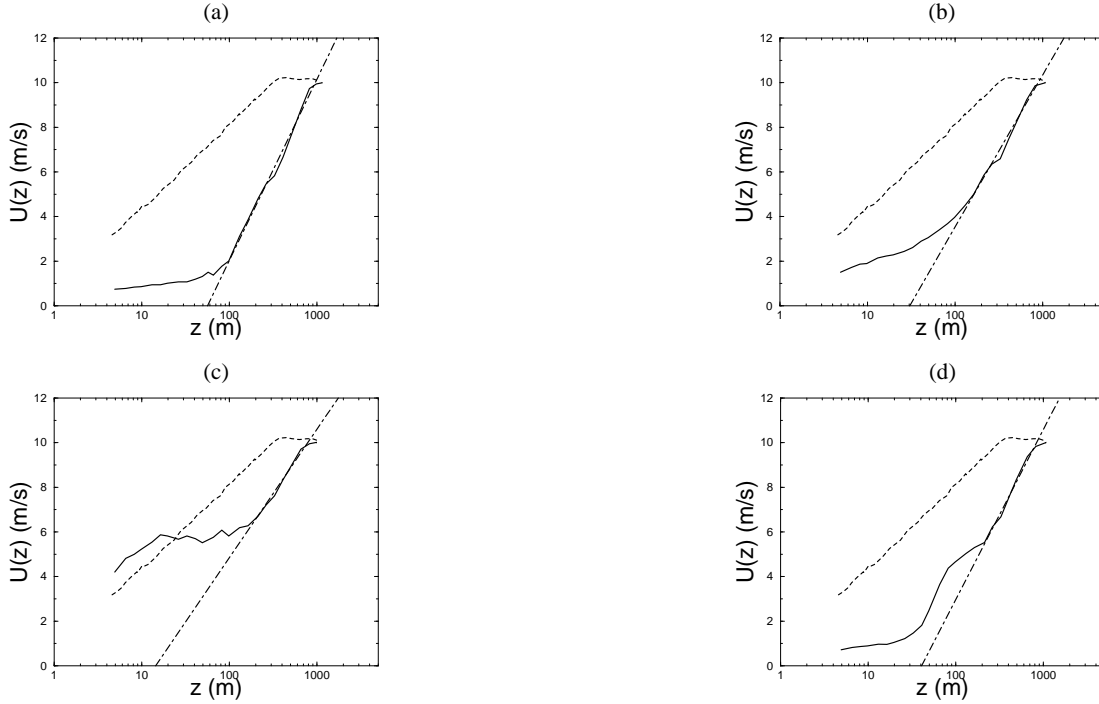


Figure 1: The local wind speed profiles $U(z)$ from the wind tunnel experiment [8] are plotted (solid lines) as a function of z for four different positions (x in Eqs. (1) and (2)) along the hill, corresponding to (a) $x = 0$, (b) $x = \lambda/4$, (c) $x = \lambda/2$ and (d) $x = 3\lambda/4$. The dashed lines represent the unperturbed profile. The dot-dashed lines represent the logarithmic law (1), with parameters $u_*^{\text{eff}}(x)$ and $z_0^{\text{eff}}(x)$ obtained by least-square fits performed inside the scaling regions. The values of these effective parameters are given in the text.

the wind tunnel experiments. This can be easily seen in Fig. 1 (the analogous of Fig. 1 in Ref. [6]), where typical behaviours for the horizontal wind speed profile $U(z)$ (see Eq. (1); for the sake of brevity, the dependence on the x -coordinate is omitted in the notation

from now on) as a function of z are presented in lin-log coordinates for the rough case and for four values of the x -coordinate corresponding to: (a) $x = 0$ (i.e. $h = 0$), (b) $x = \lambda/4$ (i.e. $h = H/2$ upwind), (c) $x = \lambda/2$ (i.e. $h = H$) and (d) $x = 3\lambda/4$ (i.e. $h = H/2$ downwind), respectively. Similar behaviours have been found (but not reported here for the sake of brevity) also for the smooth case. From this figure, clean logarithmic region of the type described by Eq. (1) are evident and both $u_\star^{\text{eff}}(x)$ and $z_0^{\text{eff}}(x)$ can be measured by least-square fits. Specifically, for the four above positions along the hill, we have obtained the following values of $u_\star^{\text{eff}}(x)$ and $z_0^{\text{eff}}(x)$: 1.73 m/s, 0.053 m (for $h = 0$); 1.38 m/s, 0.028 m (for $h = H/2$ upwind); 0.95 m/s, 0.007 m (for $h = H$) and 1.27 m/s, 0.022 m (for $h = H/2$ downwind), respectively. Such values can be compared with those in the absence of any hill: $u_\star \sim 0.62$ m/s and $z_0 \sim 0.66$ m.

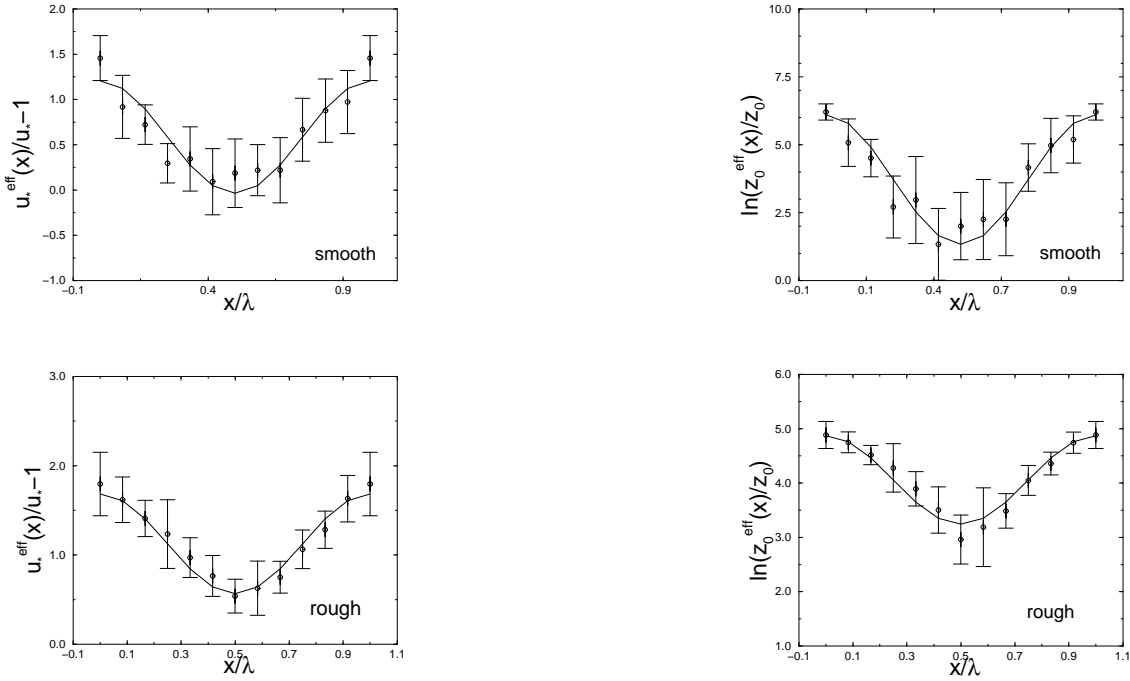


Figure 2: The measured (circles) effective parameters $u_\star^{\text{eff}}(x)/u_\star - 1$ (on the left) and $\ln(z_0^{\text{eff}}(x)/z_0)$ (on the right) as a function of the ratio x/λ along the axis of the hill in the smooth case (above) and in the rough case (below). The continuous lines represent the sinusoidal law best-fitting the experimental data.

The results of the least-square fits are summarized in Fig. 2 where both profiles $u_\star^{\text{eff}}(x)/u_\star - 1$ (on the left) and $\ln(z_0^{\text{eff}}(x)/z_0)$ (on the right) are shown as a function of x/λ for both the smooth (above) and the rough (below) case (different scales in the or-

dinates have been adopted). Notice that both $u_{\star}^{\text{eff}}(x)/u_{\star} - 1$ and $\ln(z_0^{\text{eff}}(x)/z_0)$ have been fitted with the analytical expression (2), relative to the topographic profile, but with a shift of $\lambda/2$ (i.e. $x \mapsto x + \lambda/2$ in (2)). More precisely, we suggest the expression:

$$y(x) = \langle y \rangle - A_y [h(x)/H - 1/2] \quad (3)$$

where $y(x)$ stays for either $u_{\star}^{\text{eff}}(x)/u_{\star} - 1$ or $\ln(z_0^{\text{eff}}(x)/z_0)$, $\langle y \rangle$ is the average value of $y(x)$ in the interval $(0, \lambda)$ and $h(x) \equiv h(x, y)$ is the topographic shape given in Eq. (2). It should be also stressed that we have considered $\ln(z_0^{\text{eff}}(x)/z_0)$ instead of the simpler ratio $z_0^{\text{eff}}(x)/z_0$, because the former parameter is more similar to the topography shape than the second one.

It is now interesting to put together the new results here obtained with those of Ref. [6]. This allows to investigate at which degree of accuracy one can express the behaviours of quantities like the average values, $\langle y \rangle$, and amplitudes, A_y , of these sinusoidal shapes solely in terms of simple geometrical parameters. Simple considerations suggest to look at the ratio H/λ : this is indeed a rough measure of the hill slope.

The values of $\langle y \rangle$ are reported in Fig. 3 for both the smooth and the rough case. The



Figure 3: The mean values $\langle u_{\star}^{\text{eff}}(x)/u_{\star} \rangle - 1$ and $\langle \ln(z_0^{\text{eff}}(x)/z_0) \rangle$ in Eq. (3) versus H/λ . Stars are relative to the Wood and Mason numerical simulations ($u_{\star} \sim 0.44 \text{ m/s}$, $z_0 \sim 0.16 \text{ m}$); diamonds are relative to the smooth case ($u_{\star} \sim 0.43 \text{ m/s}$, $z_0 \sim 0.05 \text{ m}$) and squares are relative to the rough case ($u_{\star} \sim 0.62 \text{ m/s}$, $z_0 \sim 0.66 \text{ m}$). Dashed lines represent the linear curve best-fitting the Wood and Mason numerical data.

dashed lines (a linear fit in H/λ) are obtained considering only the results of numerical simulations, while the values from the wind tunnel experiments are reported with their error bars. These monotonic behaviours are expected on account of the increasing of the (total) transfer of momentum towards the surface arising for increasing slopes. The amplitudes A_y are shown in Fig. 4. The dashed lines are a parabolic fit in H/λ and, as for $\langle y \rangle$, they have been obtained by only considering the results of the numerical simulations.

The values from the wind tunnel experiments are again presented in the same figure. Curves relative to the amplitudes reach a maximum for $H/\lambda \sim 0.20$, after that start to decrease. We can argue that two different mechanisms exist and act in competition. The physical key role is played by curvature effects [12], already invoked in Ref. [6] to explain the presence of minima (maxima) located above the hill top (valley) for both $u_{\star}^{\text{eff}}(x)$ and $\ln z_0^{\text{eff}}(x)$. To be more specific, let us consider the two opposite limits $H/\lambda \ll 1$ and $H/\lambda \gg 1$, from which we can easily isolate the two competing mechanisms. Concerning the former limit, we have gentle slopes and it is well known that in this case the flow closely follows the surface contour. Streamlines are (weakly) curved and, as pointed out in Ref. [12], energy is transferred towards the large scale components above the hill tops, while it blows towards the smaller scales above the valleys. The quantity $u_{\star}^{\text{eff}2}(x)$, that is a measure of the energy of turbulence, is thus smaller on the hill top than above the valley. Let us increase (just a little bit) H/λ . The flow again closely follows the surface contour but streamlines are now more curved. As pointed out in Ref. [12], energy transfer thus increases and, as an immediate consequence, the same happens for the difference between the maximum and the minimum of $u_{\star}^{\text{eff}}(x)$. But this means an augmentation of its modulation amplitude.

In the second limit $H/\lambda \gg 1$, a further important effect arises due to trapping regions placed on the downstream hill slopes. It is in fact well known (see, e.g., [13]) that, for surface slopes large enough, the flow is not able to follow the contour surface and separates. In this case, in between two hill crests, the flow is essentially trapped and, roughly speaking, streamlines are expunged in the wake region. The dynamical consequence is that the flow streamlines are weakly modulated, and this also happens for the shape of $u_{\star}^{\text{eff}}(x)$. If we now decrease the ratio H/λ , trapping effects reduce and this means that the wake can penetrate more deeply in the valley, with the consequent increasing of curvature effects and thus of the $u_{\star}^{\text{eff}}(x)$ amplitude.

From the inspection of these two limits, it is thus clear that a maximum in the amplitude should be attained for a certain finite value of H/λ , i.e. when the two competing mechanisms are balanced.

Being the maximum (minimum) of $\ln z_0^{\text{eff}}(x)$ directly related to the presence of the maximum (minimum) of $u_{\star}^{\text{eff}}(x)$ (see Ref. [6] for the discussion of this point) the argumentations above presented hold also for $\ln z_0^{\text{eff}}(x)$.

Comparing the values of both amplitudes and mean values of the effective parameters extrapolated from the numerical simulations (i.e. from the linear fits in Figs. 3 and 4) and those from the wind tunnel experiments, we notice that, for the smooth case, experiments are always compatible (within the error bars) with the numerical simulations. This is not always the case for the rough case. We remark that u_{\star} and z_0 (relative to the flat terrain) are closer to the WM93 case studies in the smooth case than in the rough case. This suggest that the expression of both amplitudes and mean values solely in terms of

geometrical quantities like the ratio H/λ is a reasonable approximation for small variations of the ‘bare’ parameters u_* and z_0 . When the range of variability of the latter two parameters increases, an explicit dependence on them has to be taken into account.



Figure 4: The values of the amplitude A_y in Eq. (3) relative to $y = u_*^{eff}(x)/u_* - 1$ and $y = \ln(z_0^{eff}(x)/z_0)$ versus H/λ . Stars are relative to the Wood and Mason numerical simulations ($u_* \sim 0.44$ m/s, $z_0 \sim 0.16$ m), diamonds are relative to the smooth case ($u_* \sim 0.43$ m/s, $z_0 \sim 0.05$ m) and squares are relative to the rough case ($u_* \sim 0.62$ m/s, $z_0 \sim 0.66$ m).

For a better evaluation and understanding of the dependence of $\langle y \rangle$ and A_y on H/λ , z_0 and u_* , the analysis of more numerical and wind tunnel experiments, and possibly in nature, is necessary. Nevertheless, the wind tunnel data here considered give a strong confirmation of the existence of a pre-asymptotic regime characterized by a generalized law-of-the-wall given by Eq. (1) and pointed out for the first time in Ref. [6]. Thus, this phenomenon appears as a real physical property and not a spurious feature produced by some of the approximations (e.g. parameterizations of small-scale, unresolved dynamics) used to solve the Navier-Stokes equations.

Acknowledgements We are particularly grateful to P.A. Taylor for providing us with his data-set relative to the wind tunnel experiments as well as many useful comments and discussions. Helpful discussions and suggestions by E. Fedorovich, D. Mironov, G. Solari, F. Tampieri and S. Zilitinkevich are also acknowledged.

References

- [1] P.A. Taylor, Model prediction of neutrally stratified planetary boundary layer flow over ridges, Q.J.R. Meteorol. Soc., 107, 111-120 (1981).

- [2] S.E. Belcher, T.M.J. Newley and J.C.R. Hunt, The drag on an undulating surface induced by the flow of a turbulent boundary layer, *J. Fluid Mech.*, 249, 557-596 (1993).
- [3] S. Emeis, Pressure drag of obstacles in the atmospheric boundary layer, *J. Appl. Meteorol.*, 29, 461-476 (1990).
- [4] N. Wood and P. Mason, The pressure force induced by neutral, turbulent flow over hills. *Q.J.R. Meteorol. Soc.*, 119, 1233-1267 (1993).
- [5] D. Xu and P.A. Taylor, Boundary-Layer Parameterization of Drag over Small Scale Topography *Q.J.R. Meteorol. Soc.*, 121, 433-443 (1995).
- [6] S. Besio, A. Mazzino and C.F. Ratto, Local log-law of the wall: numerical evidences and reasons, *Phys. Lett. A*, 275, 152-158 (2000).
- [7] A.S. Monin and A.M. Yaglom, *Statistical Fluid Mechanics*, (MIT Press, Cambridge, Mass., 1975).
- [8] W. Gong, P.A. Taylor and A. Dornbrack, Turbulent boundary-layer flow over fixed aerodynamically rough two-dimensional sinusoidal waves, *Bound. Layer Meteorol.*, 312, 1-37 (1996).
- [9] M. Shokr and H.W. Teunissen, Use of hot-wire anemometry in the AES boundary-layer wind tunnel with particular reference to flow over hill models, Res. Rep. MSRB 88-9, 4905 Dufferin Street, Downsview, Ontario, Canada.
- [10] S. Finardi, G. Brusasca, M.G. Morselli, F. Trombetti and F. Tampieri, Boundary-layer flow over analytical two-dimensional hills: a systematic comparison of different models with wind tunnel data, *Bound. Layer Meteorol.*, 63, 259-291 (1993).
- [11] E. Canepa, E. Georgieva, A. Mazzino and C.F. Ratto, Comparison between the results of a new version of the AVACTA II atmospheric diffusion model and tracer experiments, *Il Nuovo Cimento C*, 20, 461 (1997).
- [12] A.A. Townsend, *The structure of turbulent shear flow* (Cambridge University Press, Cambridge, 1980).
- [13] L.M. Milne-Thomson, *Theoretical hydrodynamics* (MacMillan & Co, London 1968).